Turbulence modification by inertial particles and its influence on the spectral energy budget in planar Couette flow

David H. Richter

Citation: Physics of Fluids **27**, 063304 (2015); doi: 10.1063/1.4923043
View online: http://dx.doi.org/10.1063/1.4923043
View Table of Contents: http://scitation.aip.org/content/aip/journal/pof2/27/6?ver=pdfcov
Published by the AIP Publishing

PHYSICS OF FLUIDS **27**, 063304 (2015)

Turbulence modification by inertial particles and its influence on the spectral energy budget in planar Couette flow

David H. Richter
Department of Civil and Environmental Engineering and Earth Sciences, University of Notre Dame, Notre Dame, Indiana 46556, USA

(Received 11 December 2014; accepted 15 June 2015; published online 29 June 2015)

Two-way coupled, particle-laden simulations are performed in turbulent Couette flow with the purpose of investigating the spectral extent of the particle influence on the turbulent energy cascade in wall-bounded flows. Direct numerical simulation of the carrier phase is performed in conjunction with the Lagrangian point-particle approximation for particles of three distinct inertia ranges: $St_K = [O(1), O(10), O(100)]$. Simulations are also performed at three increasing Reynolds numbers ($Re_\tau \approx [125, 325, 900]$) to determine the longevity of these effects as the scale separation between large and small motions is increased. A spectral decomposition of the turbulent kinetic energy (TKE) budget shows that two simultaneous effects of particles are occurring: first, the mere presence of particles causes a reduction of TKE production across nearly the entire wavenumber range, where the particle Stokes number only determines the magnitude of this reduction; second, the direct energy exchange term between the carrier and dispersed phases is relatively small in magnitude compared to changes in production; however, its location in wavenumber space is highly dependent on Stokes number and is influenced heavily by preferential concentration. The combined effect of these distinct processes is important to consider when developing large eddy simulation (or any other) two-way coupled particle-laden turbulence parameterizations. [http://dx.doi.org/10.1063/1.4923043]

I. INTRODUCTION AND MOTIVATION

The numerical simulation of particle-laden turbulent flows has seen significant advances in recent years, yet remains a challenging problem motivated by processes spanning a wide range of scientific and industrial applications. In particular, the phenomenon of turbulence modification by a dispersed phase is a complex process which depends on many factors including particle size, particle Reynolds number, mass loading, characteristic turbulence scales, flow type, gravitational orientation, and particle inertia. Despite attempts to classify the general conditions under which to expect turbulent kinetic energy (TKE) attenuation versus TKE modulation,[1–3] the wide variety of laboratory and numerical experiments continue to reveal complex couplings between the carrier and dispersed phases.

A growing number of experimental observations in isotropic[4–8] and wall-bounded[9–11] turbulent flows have shown that even a simple description of "TKE attenuation" versus "TKE augmentation" is misleading, since not only does this classification depend on many flow parameters, but also a single flow can exhibit both attenuation and modulation depending on location in physical space[12] and wavenumber space.[13] Likewise, numerical simulations of two-way coupled, particle-laden turbulent flows have revealed complex modifications to both the production and dissipation of TKE and/or Reynolds stresses in isotropic[14–17] and wall-bounded[18–23] flows.

Based on dimensional grounds, the effects of a dilute concentration of particles whose diameters are much smaller than the Kolmogorov length of the turbulence and whose particle Reynolds numbers are small are only a function of the mass loading and particle Stokes number (defined

as the ratio of the particle acceleration time scale to some flow time scale).[16,24] For flows meeting these conditions, standard point-particle techniques have been shown in many cases to provide accurate representations of the relevant turbulence modification processes. These point particle methods, particularly in the two-way coupling context, therefore parameterize processes at the surface of the particle, including, for example, dissipation and the formation of wakes or other velocity perturbations. Models which explicitly resolve the flow surrounding each particle (so-called particle resolved models), while computationally expensive, are becoming increasingly utilized to explore systems where the point particle method assuredly fails (e.g., when particles are larger than the smallest flow scales[24–26]) as well as tests the development of dispersed phase models (including the point particle model), see for example Tenneti and Subramaniam[27] for a review of recent applications. The limitation of the particle resolved models, of course, lies in their computational expense, and for studies including the present analysis, high Reynolds numbers, and/or particle numbers preclude this as a feasible tool.

For small, heavy particles, therefore, modifications to turbulence must therefore ultimately arise from the additional drag force resulting from a slip velocity at the particle surface. Indeed, a common feature of experimental and numerical studies is a damping of turbulent fluctuations through this drag (particularly in non-streamwise directions) after the addition of small inertial particles.[9,20,22,28] However, the ability of inertial particles to depart from fluid streamlines and preferentially concentrate in high strain regions complicates a simple description of the collective effects of particle drag. For example, in many energy spectra taken from two-way coupled isotropic turbulence simulations, TKE enhancement is observed at high wavenumbers while TKE attenuation is found at low wavenumbers (e.g., see the review by Poelma and Ooms[29]). In some sense, this broad spectral influence of the dispersed phase is counterintuitive since the individual particle drag is occurring near the smallest scales of the turbulence. The modification to small-scale turbulence dissipation, however, can apparently somehow modify the motions responsible for TKE production (i.e., at large scales) and thereby adjust the entire turbulence cascade. The same wavenumber sensitivity is found in several wall-bounded studies as well,[9,13,20,30,31] while several numerical investigations show no such "crossover wavenumber."[18,22,23]

It is noteworthy that nearly all particle-laden direct numerical simulation (DNS) studies to date have been restricted to low Reynolds numbers ($Re_\tau \approx 180$ typically, based on the channel half-height and friction velocity) and therefore are limited in the range of scales with which the particles can interact. At the same time, experiments are typically done at Reynolds numbers currently difficult to achieve with DNS (e.g., Kulick *et al.*[9]), and thus, interpretation of experimental results and comparison to point-particle simulations remains problematic. Richter and Sullivan[32] therefore used DNS simulations of particle-laden planar Couette flow at friction Reynolds numbers of $Re_\tau \approx 125, 325$, and 900 to investigate the interaction of near-wall coherent structures with small, heavy particles at varying Stokes numbers, focusing on their continued influence as the flow Reynolds number became asymptotically large. Couette flow was chosen instead of the more typical turbulent channel flow because (1) the total stress across the channel remains constant with height, which is convenient for analyzing wall-normal momentum transfer and (2) in addition to the typical near-wall vortices and high/low speed streaks, Couette flow exhibits additional large-scale flow structures (herein referred to as "rollers") with distinct time and length scales on the order of the domain height. The existence of both small- and large-scale vortical structures at opposite ends of the wavenumber spectrum provides a unique case where particles of varying Stokes numbers have multiple distinct flow features with which they can interact. By suppressing near-wall hairpin structures, Richter and Sullivan[32] suggest that small-scale particle/fluid interactions disrupt the regeneration process of near-wall coherent structures, which could influence the entire energy cascade in a way not easily described solely by an additional dispersed phase energy dissipation.

The current study builds upon the work of Richter and Sullivan[32] by computing the spectral energy budget for these high Reynolds number planar Couette flows. One pertinent question which remains unanswered is regarding the collective effect of small particles on large-scale motions: can particles modify large-scale momentum and kinetic energy budgets by merely impacting small-scale motions (i.e., providing an upscale influence), or can particles interact with large-scale motions directly, perhaps through the formation of clusters much larger than an individual particle

diameter? This answer has significant implications for multiphase modeling in two-fluid (i.e., Eulerian representations of the dispersed phase) or large eddy simulations.

In this context, this study is motivated by the scales over which small, Lagrangian point-particles exert their influence, and how this changes the bulk TKE budget and resulting turbulence statistics in wall-bounded turbulent flows. The recent study of Zhao *et al.*[18] provides a detailed look at the energy transfer between the carrier and dispersed phases in a turbulent channel, and shows that while particles can extract kinetic energy from the central regions of the flow and deposit it into the near-wall buffer region, the slip velocity between the phases leads to energy dissipation and damping of spanwise and wall-normal fluctuations. Also recently, Gualtieri *et al.*[33] highlight the importance of particle clustering on TKE production in homogeneous shear flow using a spectral decomposition of the particle feedback term of the energy budget, while Druzhinin[34] performs asymptotic theory for describing this term in isotropic turbulence. In the present study, one-dimensional spectra are computed in both the streamwise and spanwise directions, and an analysis of the production and particle-induced feedback terms reveals a dual set of feedback mechanisms through which particles can modify the turbulence cascade.

As with numerous other numerical investigations of two-way coupling, we focus on the simplest representation of small particles in order to form a baseline understanding upon which to build from. The particles are assumed to be sufficiently heavy such that the hydrodynamic drag is the dominant force term in the particle evolution equation,[35] gravity is neglected to remove the complications of particle settling, and particle-particle collisions are neglected. As a result, the physical systems for which this study contributes insight are those where low volume fractions of heavy particles whose diameters are much smaller than the Kolmogorov scale of the flow interact with near-wall turbulence. These conditions are often met in geophysical and industrial applications, while care must be taken to extend the results to real systems where these basic assumptions are violated.

II. METHOD

A. Numerical procedure

As described in past studies,[23,32] the carrier phase DNS is solved using a pseudospectral method with antialiasing in the homogeneous, periodic streamwise (x_1), and spanwise (x_2) directions, while second order finite differencing is used in the inhomogeneous wall-normal (x_3) direction. The equations solved are the incompressible Navier-Stokes equations for mass and momentum conservation, modified with a particle coupling force F_i,

$$\frac{\partial u_j}{\partial x_j} = 0, \tag{1}$$

$$\frac{\partial u_i}{\partial t} + u_j \frac{\partial u_i}{\partial x_j} = -\frac{\partial p}{\partial x_i} + \nu_f \frac{\partial^2 u_i}{\partial x_j \partial x_j} + \frac{1}{\rho_f} F_i, \tag{2}$$

where ν_f is the carrier phase ("fluid") kinematic viscosity, ρ_f is the fluid density, u_i is the fluid velocity, and p is the pressure normalized by the fluid density. Equation (2) is integrated in time using a low-storage, third order Runge-Kutta (RK) scheme for all terms.[36] Incompressibility is enforced by solving a pressure Poisson equation and correcting the velocity field to guarantee a divergence free field at each RK stage. No-slip boundary conditions are employed at the domain walls, while periodicity is used in the streamwise and spanwise directions.

The particle feedback force arises from the drag of individual Lagrangian point particles within the flow. Forces other than the Stokes drag (e.g., added mass, lift, Basset history, gravity, and particle-particle collisions) are neglected since the current focus is directed towards dispersed phase systems characterized by small, heavy, noninteracting particles.[35,37] Thus, each Lagrangian particle is transported throughout the domain by integrating the following equations for each particle position $x_{p,i}$ and velocity $v_{p,i}$ in time:

$$\frac{dx_{p,i}}{dt} = v_{p,i}, \tag{3}$$

$$\frac{dv_{p,i}}{dt} = \frac{f_i}{m_p} = \left(1 + 0.15Re_p^{0.687}\right)\frac{1}{\tau_p}\left(u_{f,i} - v_{p,i}\right). \tag{4}$$

Here, m_p is the mass of the particle, f_i is the drag force felt by an individual particle, τ_p is the particle Stokes acceleration time scale ($\tau_p = \frac{\rho_p d_p^2}{18\mu_f}$), where d_p is the particle diameter, and $u_{f,i}$ is the fluid velocity interpolated to the particle location using sixth-order Lagrange polynomials. The term containing Re_p (the particle Reynolds number: $Re_p = \frac{d_p|v_{p,i}-u_{f,i}|}{\nu_f}$) is a Reynolds number correction to the Stokes drag,[38] although the average particle Reynolds numbers rarely exceed $O(1)$. The coupling force F_i is computed by linearly projecting the negative of each individual particle force ($-f_i$) onto the eight surrounding nodes of the carrier flow computational grid cell. More details can be found in Richter and Sullivan.[23] It should be noted that for the present numerical setup, the order of the velocity interpolation to obtain $u_{f,i}$ (sixth order Lagrange polynomial) does not match the projection order (linear), which, as pointed out by Sundaram and Collins[39] can lead to violations of kinetic energy conservation between phases despite maintaining momentum conservation. For the present results, however, tests have been performed with trilinear interpolation for the particle velocity $u_{f,i}$ such that the interpolation schemes are symmetric, and differences in all results discussed herein are within 2%.

B. Domain and simulation parameters

Before describing the various simulation parameters, it is important to emphasize the range of validity of the current numerical experiments. By invoking the non-interacting point-particle approximation, the results described in the subsequent discussions are only applicable to physical systems where the approximation's basic conditions are met: (i) the particles are smaller than the Kolmogorov length scale of the flow, (ii) the density ratio between the dispersed phase and carrier phase is large, (iii) the particle Reynolds numbers are small (i.e., no wakes or other distortions of the surrounding velocity field), and (iv) the volume fraction is small, thus ensuring that the role of particle collisions is small. Here, the maximum bulk volume fraction of the particles is $\phi_V = 2.5 \times 10^{-3}$, and all other simulations have bulk volume fractions $O(10^{-4})$ or less. The density ratio varies between 100 and 8000, the particle Reynolds number remains O(1) or lower, and the ratio d_p/η_K is maintained at a value of approximately 0.45. The particles are assumed to bounce elastically from the walls.

Turbulent planar Couette flow develops between two infinitely parallel plates moving with equal and opposite velocity U_0 and separated by a distance H. The bulk Reynolds number of the flow, $Re_b = HU_0/\nu_f$, is varied between 8100, 24 000, and 72 000 by modifying the plate velocity U_0 and domain height H in such a way as to maintain an approximately constant Kolmogorov length at the channel centerline across all Re_b. The corresponding friction Reynolds numbers range between $Re_\tau \approx 125$ and $Re_\tau \approx 900$. The computational mesh for each respective Re_b has a grid size $[N_1 \times N_2 \times N_3]$ of $[128 \times 256 \times 128]$, $[256 \times 512 \times 256]$, and $[512 \times 1024 \times 512]$. In all cases, the domain size is specified to be $[L_1, L_2, L_3] = [2\pi H, 2\pi H, H]$. Grid stretching is employed in the x_3^+ direction so that the flow is fully resolved at the wall ($\Delta x_3^+ \approx 1$ at the wall). Note that given the linear projection operator which relates the drag force from each individual particle to the Eulerian mesh, the use of grid stretching will inherently change the vertical range of influence of each particle based on wall-normal distance. This work assumes that the influence of this wall-normal variation of particle influence is small given both the findings of Sundaram and Collins[39] (i.e., the insensitivity of energy spectra to increasing the projection stencil) as well as the smoothness of this stretching procedure.

It should also be noted that due to computational constraints, this domain size is not large enough to capture the entire streamwise extent of the large-scale Couette rollers which develop in the flow.[40] However, as shown by Tsukahara *et al.*[41] and confirmed in preliminary tests, TKE and Reynolds stress statistics are relatively insensitive to this domain restriction. Furthermore, the

TABLE I. Summary of simulation parameters: bulk Reynolds number $Re_b = HU_0/\nu_f$; friction Reynolds number $Re_\tau = Hu_\tau/2\nu_f$; bulk particle mass loading ϕ_m; bulk particle volume fraction ϕ_V; particle Stokes number St_K; particle Stokes number based on wall units St^+; ratio of particle density to fluid density ρ_p/ρ_f; number of particles N_p.

Run	Re_b	Re_τ	ϕ_m	ϕ_V	St_K	St^+	ρ_p/ρ_f	N_p
1	8 100	121	0.0	0.0				0
2	8 100	122	0.25	2.5×10^{-3}	1.2	8.2	100	1.5×10^{6}
3	8 100	124	0.25	2.5×10^{-4}	12	85	1000	1.5×10^{5}
4	8 100	122	0.25	3.1×10^{-5}	97	656	8000	1.9×10^{4}
5	24 000	325	0.0	0.0				0
6	24 000	317	0.25	2.5×10^{-3}	1.1	14	100	1.2×10^{7}
7	24 000	331	0.25	2.5×10^{-4}	9.5	152	1000	1.2×10^{6}
8	24 000	321	0.25	3.1×10^{-5}	94	1146	8000	1.5×10^{5}
9	72 000	917	0.0	0.0			0	
10	72 000	848	0.25	2.5×10^{-3}	1.1	25	100	9.6×10^{7}
11	72 000	869	0.25	2.5×10^{-4}	9.8	262	1000	9.6×10^{6}
12	72 000	911	0.25	3.1×10^{-5}	83	2307	8000	1.2×10^{6}

present goal is to characterize the general interactions of particles with distinct time and length scales which exist in the flow, regardless of whether or not these large structures are influenced by streamwise or spanwise periodicity. In subsequent discussions of the spanwise and streamwise energy spectra, any influences of the domain size will be noted.

For each Reynolds number, four simulations are performed, including one unladen case and one case for each of three different Stokes numbers at a constant mass fraction of $\phi_m = 0.25$: $St_K = O(1)$, $O(10)$, and $O(100)$, where $St_K = \tau_p/\tau_K$ is the ratio of the Stokes acceleration time scale of the particle to the Kolmogorov time scale at the channel centerline. The Stokes numbers were chosen to test a wide range of particle inertia and further characterize the influence of preferential concentration and particle mass on two-way coupling in a simplified system. Table I contains a summary of the relevant simulation data. Additional simulation and numerical method information can be found in Richter and Sullivan.[32]

C. Spectral energy budgets

A primary goal of this study is to analyze the spectral content of both the TKE and its budget in a two-way coupled, particle-laden turbulent wall flow. In particular, the spectral extent of the particle feedback force, as well as the spectral extent of TKE production modification, is of significant interest. This is of critical importance for subgrid and two-fluid modeling, since two-way coupling may manifest itself throughout the entire energy spectrum despite the particles having individual diameters smaller than the smallest length scales of the turbulence. If the dissipative effects of particles are contained at high wavenumbers, for instance, this may be favorable for subgrid modeling since a concentration-dependent dissipation may perhaps be sufficient for parameterizing the effects of particles at the unresolved scales (see for example the discussions in Sundaram and Collins,[17] where dissipation due to the slip velocity between particle and fluid appears as an extra source of dissipation in isotropic turbulence). If the preferential arrangement of particles into clusters, however, dictates the scales over which the energy budget is modified, this would pose a much more challenging parameterization requirement. The present goal is to characterize the spectral extent of particle modification, while model and parameterization development is left for future work.

Since the flow is homogeneous but not isotropic in a given horizontal plane, one-dimensional spectra are taken independently in the streamwise and spanwise directions. This is opposed to performing a two-dimensional spectral decomposition at each height z, which has been previously done for unladen turbulent channel flows (e.g., Bolotnov *et al.*,[42] Domaradzki[43]). In these cases, the

streamwise wavenumber will be referred to as k_1 and the spanwise wavenumber will be referred to as k_2.

To derive the spectral energy budget equations, the flow velocity and pressure are first decomposed into their mean (capital) and fluctuating (prime) quantities: $u_i = U_i + u_i'$ and $p = P + p'$. Then, the fluctuating quantities are expressed as their discrete Fourier series in either the x_1 or x_2 directions (shown only for the fluctuating fluid velocity, same for pressure),

$$u_i'(x_1, x_2, x_3, t) = \sum_{k_1} \hat{u}_i'(k_1, x_2, x_3, t) e^{ik_1 x_1} \tag{5}$$

or

$$u_i'(x_1, x_2, x_3, t) = \sum_{k_2} \hat{u}_i'(x_1, k_2, x_3, t) e^{ik_2 x_2}, \tag{6}$$

where, using the notation of Bolotnov *et al.*[42] and Pope[44] (p. 207), the Fourier coefficients are given as either

$$\hat{u}_i'(k_1, x_2, x_3, t) = \mathcal{F}_{k_1}\{u'(x_1, x_2, x_3, t)\} \tag{7}$$

or

$$\hat{u}_i'(x_1, k_2, x_3, t) = \mathcal{F}_{k_2}\{u'(x_1, x_2, x_3, t)\}. \tag{8}$$

$\mathcal{F}_{k_1}$ and $\mathcal{F}_{k_2}$ (or $\mathcal{F}_{k_\alpha}$ in general, where $\alpha = 1$ or 2; no summations implied throughout) refer to discrete Fourier transforms in the x_1 and x_2 directions, respectively.

After decomposing the velocity and pressure into mean and fluctuating quantities, Equation (2) is then Fourier transformed, resulting in equations either for $\hat{u}_i'(k_1, x_2, x_3, t)$,

$$\begin{aligned}
&\frac{\partial \hat{u}_i'}{\partial t} + \hat{u}_3' \frac{\partial U_i}{\partial x_3} + ik_1 \hat{u}_i' U_1 \\
&\quad + ik_1 \sum_{k_1'} \hat{u}_i(k_1') \hat{u}_1'(k_1 - k_1') + \frac{\partial}{\partial x_2}\left[\sum_{k_1'} \hat{u}_i(k_1') \hat{u}_2'(k_1 - k_1')\right] + \frac{\partial}{\partial x_3}\left[\sum_{k_1'} \hat{u}_i(k_1') \hat{u}_3'(k_1 - k_1')\right] \\
&\qquad = -ik_1 \hat{p}' \delta_{i1} - \frac{\partial \hat{p}'}{\partial x_2}\delta_{i2} - \frac{\partial \hat{p}'}{\partial x_3}\delta_{i3} - \nu_f |k_1|^2 \hat{u}_i' + \frac{\partial^2 \hat{u}_i'}{\partial x_2^2} + \frac{\partial^2 \hat{u}_i'}{\partial x_3^2} + \frac{1}{\rho_f}\hat{F}_i
\end{aligned} \tag{9}$$

or $\hat{u}_i'(x_1, k_2, x_3, t)$,

$$\begin{aligned}
&\frac{\partial \hat{u}_i'}{\partial t} + \hat{u}_3' \frac{\partial U_i}{\partial x_3} + U_1 \frac{\partial \hat{u}_i'}{\partial x_1} \\
&\quad + \frac{\partial}{\partial x_1}\left[\sum_{k_2'} \hat{u}_i(k_2') \hat{u}_1'(k_2 - k_2')\right] + ik_2 \sum_{k_2'} \hat{u}_i(k_2') \hat{u}_2'(k_2 - k_2') + \frac{\partial}{\partial x_3}\left[\sum_{k_2'} \hat{u}_i(k_2') \hat{u}_3'(k_2 - k_2')\right] \\
&\qquad = -\frac{\partial \hat{p}'}{\partial x_1}\delta_{i1} - ik_2 \hat{p}' \delta_{i2} - \frac{\partial \hat{p}'}{\partial x_3}\delta_{i3} + \frac{\partial^2 \hat{u}_i'}{\partial x_1^2} - \nu_f |k_2|^2 \hat{u}_i' + \frac{\partial^2 \hat{u}_i'}{\partial x_3^2} + \frac{1}{\rho_f}\hat{F}_i.
\end{aligned} \tag{10}$$

For clarity, the dependencies of $\hat{u}_i'$, $\hat{p}'$, and $\hat{F}_i'$ have been suppressed except within the convective terms. Note too that the structure of the mean velocity ($U_i = [U_1(x_3), 0, 0]$) and statistical homogeneity in the x_1 and x_2 directions have been used to simplify the equations. In Equations (9) and (10), the nonlinear term $\mathcal{F}_{k_\alpha}\left\{\frac{\partial}{\partial x_j}(u_i' u_j')\right\}$ appears as a summation over all wavenumbers since products become convolutions under a Fourier transform, δ_{ij} refers to the Kronecker delta which is zero unless $i = j$, and $|k_\alpha|^2$ refers to the magnitude of the spanwise or streamwise wavenumber.

The goal is then to derive the equation governing the spectral component of the turbulent kinetic energy $\hat{E}_1(k_1, x_3)$ or $\hat{E}_2(k_2, x_3)$ (assumed averaged over both time and the x_2 and x_1 directions, respectively), which are related to the height-dependent turbulent kinetic energy $k(x_3)$,

$$k(x_3) = \frac{1}{2}\left\langle u_i'(x_1,x_2,x_3,t)u_i'(x_1,x_2,x_3,t)\right\rangle = \sum_{k_1}\hat{E}_1(k_1,x_3) = \sum_{k_2}\hat{E}_2(k_2,x_3). \tag{11}$$

Equation (11) merely states that summing the individual modes of the turbulent kinetic energy, either decomposed into streamwise or spanwise modes, will recover the total turbulent kinetic energy k, which is only a function of wall-normal distance x_3. Note that since k is written as a sum of modes $\hat{E}_1$ or $\hat{E}_2$ rather than the integral over wavenumbers, the units of $\hat{E}_1$ and $\hat{E}_2$ are length squared per time squared.

Since by definition $\hat{E}_\alpha = \frac{1}{2}\left\langle \hat{u}_i'\hat{u}_i'^*\right\rangle$, where $[\ ]^*$ refers to the complex conjugate, equations governing $\hat{E}_1(k_1,x_3)$ and $\hat{E}_2(k_2,x_3)$ are obtained by, respectively, multiplying Equations (9) and (10) by $\hat{u}_i'^*(k_1,x_2,x_3,t)$ and $\hat{u}_i'^*(x_1,k_2,x_3,t)$, averaging, and taking the real part,

$$\frac{\partial \hat{E}_1}{\partial t} = 0 = \hat{\mathcal{P}}_1(k_1,x_3) + \hat{\mathcal{T}}_1(k_1,x_3) - \hat{\epsilon}_1(k_1,x_3) + \hat{\Psi}_1(k_1,x_3), \tag{12}$$

where

$$\hat{\mathcal{P}}_1 = -\frac{\partial U_1}{\partial x_3}\mathbb{R}\left\langle \hat{u}_1'\hat{u}_3'^*\right\rangle, \tag{13}$$

$$\begin{aligned}\hat{\mathcal{T}}_1 = &-\mathbb{R}\left\langle ik_1\hat{u}_i'^*\sum_{k_1'}\hat{u}_i'(k_1')\hat{u}_1'(k_1-k_1')\right\rangle - \mathbb{R}\left\langle \hat{u}_i'^*\frac{\partial}{\partial x_2}\sum_{k_1'}\hat{u}_i'(k_1')\hat{u}_2'(k_1-k_1')\right\rangle \\ &- \mathbb{R}\left\langle \hat{u}_i'^*\frac{\partial}{\partial x_3}\sum_{k_1'}\hat{u}_i'(k_1')\hat{u}_3'(k_1-k_1')\right\rangle - \mathbb{R}\left\langle ik_1\hat{u}_1'^*\hat{p}' + \hat{u}_2'^*\frac{\partial \hat{p}'}{\partial x_2} + \hat{u}_3'^*\frac{\partial \hat{p}'}{\partial x_3}\right\rangle + \nu_f\frac{\partial^2\hat{E}_1}{\partial x_3^2},\end{aligned} \tag{14}$$

$$\hat{\epsilon}_1 = 2\nu_f|k_1|^2\hat{E}_1 + \nu_f\left\langle \frac{\partial \hat{u}_i'^*}{\partial x_2}\frac{\partial \hat{u}_i'}{\partial x_2}\right\rangle + \nu_f\left\langle \frac{\partial \hat{u}_i'^*}{\partial x_3}\frac{\partial \hat{u}_i'}{\partial x_3}\right\rangle, \tag{15}$$

$$\hat{\Psi}_1 = \mathbb{R}\left\langle \frac{1}{\rho_f}\hat{u}_i'^*\hat{F}_i\right\rangle. \tag{16}$$

Likewise for $\hat{E}_2$,

$$\frac{\partial \hat{E}_2}{\partial t} = 0 = \hat{\mathcal{P}}_2(k_2,x_3) + \hat{\mathcal{T}}_2(k_2,x_3) - \hat{\epsilon}_2(k_2,x_3) + \hat{\Psi}_2(k_2,x_3), \tag{17}$$

where

$$\hat{\mathcal{P}}_2 = -\frac{\partial U_1}{\partial x_3}\mathbb{R}\left\langle \hat{u}_1'\hat{u}_3'^*\right\rangle, \tag{18}$$

$$\begin{aligned}\hat{\mathcal{T}}_2 = &-\mathbb{R}\left\langle \hat{u}_i'^*\frac{\partial}{\partial x_1}\sum_{k_2'}\hat{u}_i'(k_2')\hat{u}_1'(k_2-k_2')\right\rangle - \mathbb{R}\left\langle ik_2\hat{u}_i'^*\sum_{k_2'}\hat{u}_i'(k_2')\hat{u}_2'(k_2-k_2')\right\rangle \\ &- \mathbb{R}\left\langle \hat{u}_i'^*\frac{\partial}{\partial x_3}\sum_{k_2'}\hat{u}_i'(k_2')\hat{u}_3'(k_2-k_2')\right\rangle - \mathbb{R}\left\langle \hat{u}_1'^*\frac{\partial \hat{p}'}{\partial x_1} + ik_2\hat{u}_2'^*\hat{p}' + \hat{u}_3'^*\frac{\partial \hat{p}'}{\partial x_3}\right\rangle + \nu_f\frac{\partial^2\hat{E}_2}{\partial x_3^2},\end{aligned} \tag{19}$$

$$\hat{\epsilon}_2 = 2\nu_f|k_2|^2\hat{E}_2 + \nu_f\left\langle \frac{\partial \hat{u}_i'^*}{\partial x_1}\frac{\partial \hat{u}_i'}{\partial x_1}\right\rangle + \nu_f\left\langle \frac{\partial \hat{u}_i'^*}{\partial x_3}\frac{\partial \hat{u}_i'}{\partial x_3}\right\rangle, \tag{20}$$

$$\hat{\Psi}_2 = \mathbb{R}\left\langle \frac{1}{\rho_f}\hat{u}_i'^*\hat{F}_i\right\rangle. \tag{21}$$

Here and throughout, angle brackets $\langle\cdot\rangle$ refer to averages both in time and over the non-Fourier-transformed horizontal direction. Summations over repeated indices in all three directions (1,2,3) are implied.

In order of terms on the right hand side of Equations (12) and (17), the first refers to shear production of kinetic energy at the specified wavenumber; the second refers to the total spectral transfer of TKE (a combination of triad interactions, viscous diffusion, and pressure fluctuations); the third refers to viscous dissipation of TKE at the specified wavenumber; and the fourth is the spectral particle coupling contribution.

Finally, by either summing Equation (12) over the streamwise wavenumbers or Equation (17) over spanwise wavenumbers, the standard budget of TKE as a function of height can be recovered,

$$0 = -\langle u_1' u_3' \rangle \frac{\partial U_1}{\partial x_3} - \frac{\partial}{\partial x_3}\left[\langle u_3' k \rangle + \langle u_3' p' \rangle - \nu_f \frac{\partial k}{\partial x_3}\right] - \nu_f \left\langle \frac{\partial u_i'}{\partial x_j}\frac{\partial u_i'}{\partial x_j}\right\rangle + \frac{1}{\rho_f}\langle u_i' F_i \rangle$$
$$= \mathcal{P}(x_3) + \mathcal{T}(x_3) - \epsilon(x_3) + \Psi(x_3). \tag{22}$$

Again, statistical homogeneity in time and in both horizontal directions has been implemented. The terms in Equation (22), in order of the terms on the right hand side, respectively, correspond to shear production $\mathcal{P}$, transport $\mathcal{T}$ (turbulent, pressure, and viscous), viscous dissipation ϵ (actually the "pseudo-dissipation," see Pope[44]), and particle contribution to TKE Ψ.

III. RESULTS AND DISCUSSION

A. Wall-normal TKE budget

Starting with the TKE budget of Equation (22), Figure 1 shows the vertical profiles of the normalized turbulent kinetic energy k for all Reynolds and Stokes numbers. Here and throughout, the superscript $[\,]^+$ refers to scaling with viscous wall units u_τ, δ_ν, and τ_ν. k is normalized by the square of the plate velocity difference U_0^2.

Figure 1 encapsulates the inherent difficulty of prescribing a description of "TKE attenuation" versus "TKE augmentation," since, among other factors, this may be a strong function of wall-normal height depending on Stokes and Reynolds numbers. At the lowest Reynolds number, for example, little change is found in k for $St_K = O(1)$ relative to the unladen case, while $St_K = O(100)$ particles slightly damp turbulent kinetic energy throughout the entire domain half-height. This seemingly contradicts the observations that $St_K = O(1)$ particles maximize preferential accumulation near the walls[45] and thus modifications to near-wall coherent structures and

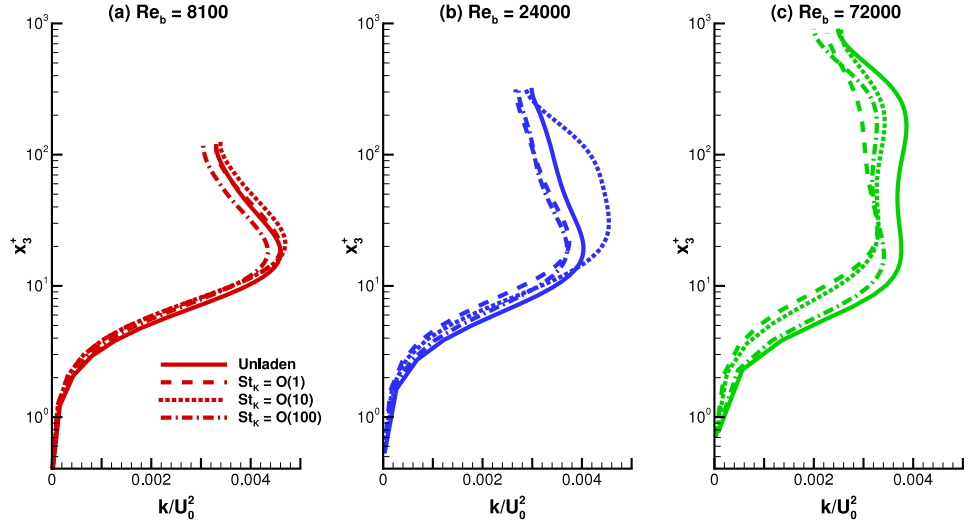

FIG. 1. Profiles of k/U_0^2 versus wall-normal height x_3^+ over the lower half of the domain for (a) $Re_b = 8100$, (b) $Re_b = 24\,000$, and (c) $Re_b = 72\,000$. Solid lines refer to the unladen cases, dashed lines to the $St_K = O(1)$ cases, dotted lines to the $St_K = O(10)$ cases, and dashed-dotted lines to the $St_K = O(100)$ cases.

Reynolds stresses,[23,32] with decreasing effectiveness at increasing Stokes numbers. Furthermore, the $St_K = O(10)$ particles damp TKE below $x_3^+ \approx 11$, yet enhance it above.

At $Re_b = 24\,000$, the picture is similar, except that the $St_K = O(1)$ particles now damp k nearly to the same degree as the $St_K = O(100)$ particles throughout most of the domain, while the TKE enhancement of the $St_K = O(10)$ particles is more pronounced. Finally, at the highest Reynolds number, the $St_K = O(10)$ particles no longer enhance TKE (and instead damp), while the $St_K = O(1)$ particles exhibit the strongest TKE attenuation over nearly the entire domain half-height.

The trends in Figure 1 can be broadly explained as follows. In turbulent Couette flow, the canonical near-wall structures of channel and boundary layer flow are found: high- and low-speed streaks, hairpin packets, quasi-streamwise vortices, etc. Simultaneously, large-scale turbulent motions which scale on the domain height H (the Couette rollers) create qualitatively similar near-wall convergence zones (i.e., streaks), but on far-removed (larger) length and (slower) time scales.[40,41] These lead to low-speed "streaks" which, unlike those in channel and boundary layer flows, span the entire length of the simulated domain and have a characteristic spanwise wavelength of roughly $3 - 4H$. These are clearly visible in the instantaneous snapshots of Figure 2 both at $x_3^+ = 10$ and $x_3^+ = 80$ when $Re_b = 24\,000$. The $St_K = O(1)$ particles, at all Reynolds numbers, have time scales near those of the traditional near-wall structures and thus accumulate in the small-scale near-wall streaks and weaken the motions responsible for them (see Figures 2(a) and 2(b) and Richter and Sullivan[32]). The $St_K = O(10)$ particles, however, have too much inertia to successfully accumulate on these scales, but instead have acceleration time scales associated with the Couette rollers and therefore accumulate in the large-scale convergence zones (see Figures 2(c) and 2(d)). The $St_K = O(100)$ particles do not experience strong preferential accumulation since their inertial time scale is longer than any available time scale in the flow (Figures 2(e) and 2(f)).

Oversimplifying somewhat (and drawing from the phenomenological evidence described for example in Richter and Sullivan,[23] Richter and Sullivan,[32] and Lee and Lee[46]), the collection of particles into either the large- or small-scale upwelling (i.e., low-speed) streaks increases the streamwise velocity fluctuation variance $\langle u_1'^2 \rangle$ by bringing their relatively low momentum from the near-wall regions and thus increasing their strength (see Figure 3). In some regions of Figure 3, the streamwise velocity fluctuations are damped, particularly at the highest Reynolds number, but this is mostly due to a shift in the wall-normal location of the variance peak. At the same time, the accumulation process damps the wall-normal and spanwise velocity fluctuations $\langle u_2'^2 \rangle$ and $\langle u_3'^2 \rangle$ associated with near-wall structures and weakens their contribution to the total TKE (see Figure 4 for wall-normal fluctuations). Similar effects have been seen in several experimental and numerical studies on channel flow.[12,19,22]

The behavior of k in Figure 1, therefore, is a balance between the strengthening of streamwise fluctuations and damping of wall-normal and spanwise fluctuations for all different Stokes and Reynolds numbers. $St_K = O(100)$ particles, for example, do not collect in any streaks and thus show only TKE attenuation at all Reynolds numbers through their collective, homogeneously distributed drag forces. The $St_K = O(10)$ particles accumulate in the large-scale convergence zones, which themselves are not confined to near-wall regions, and thus, the strengthening of these large-scale streaks wins out over wall-normal and spanwise velocity fluctuation damping in the channel center, but not at the walls (see particularly Figures 3(b) and 4(b)). At the highest Reynolds number, it is the strong attenuation of wall-normal and spanwise velocity fluctuations that dictates the overall behavior of k throughout the domain height. At the lower Reynolds numbers, this is only true at sufficiently close distances to the wall.

The current focus, however, is on the TKE budget and its subsequent spectral decomposition. Figure 5 shows the vertical profiles of each of the terms in the TKE budget of Equation (22): production $\mathcal{P}$, dissipation $-\epsilon$, transport $\mathcal{T}$, and particle contribution Ψ. Generally speaking, Figure 5 shows that TKE is produced primarily in the buffer region, with a peak of $\mathcal{P}$ occurring around $x_3^+ \approx 10$ for all Reynolds numbers. This is typical of wall-bounded turbulent flows (see Smits *et al.*,[47] for example). The transport term $\mathcal{T}$ then removes TKE from this location and brings it towards the wall to be dissipated. Significant TKE dissipation occurs both at the location of

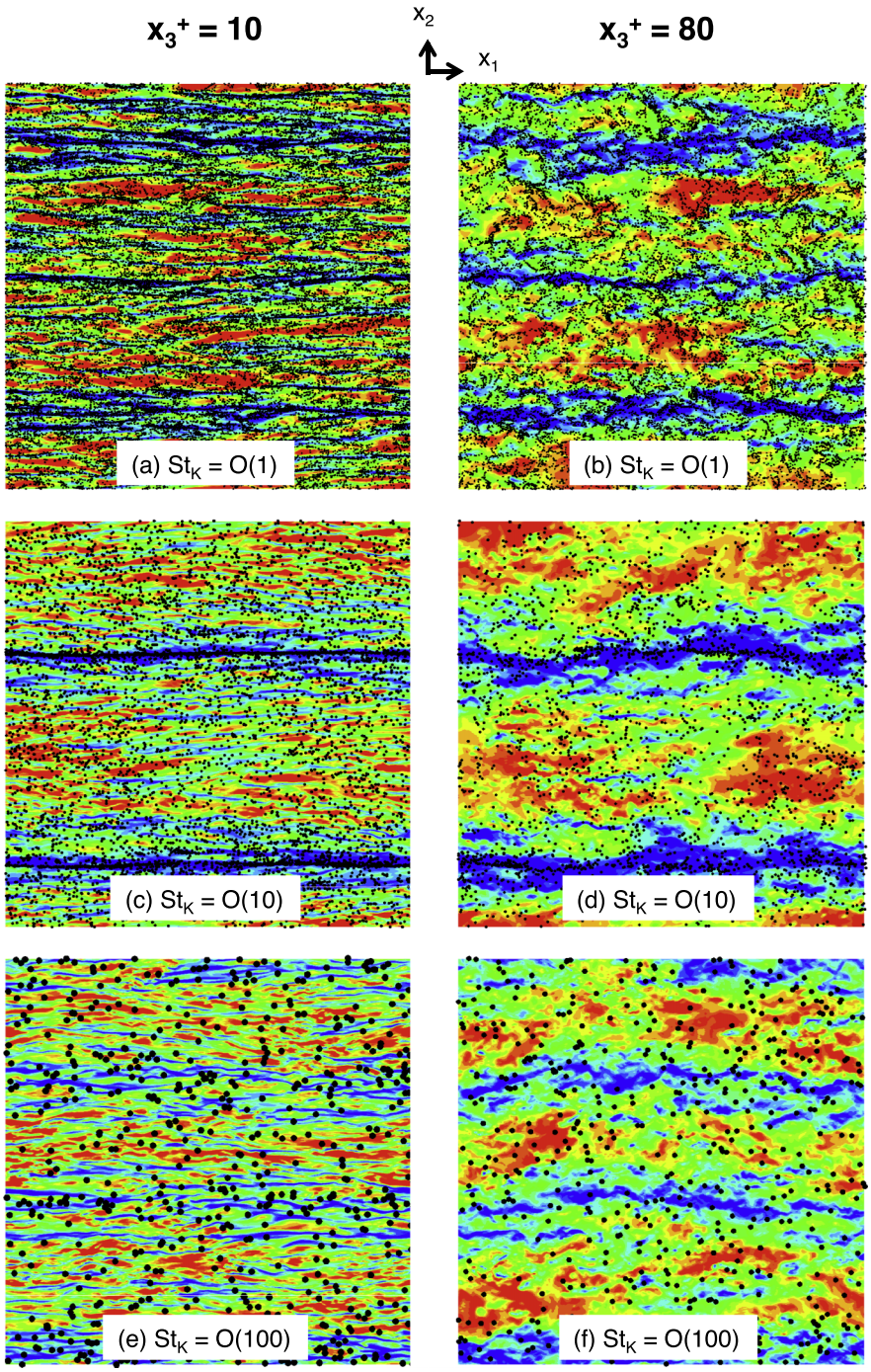

FIG. 2. Contours of instantaneous streamwise velocity fluctuations u_1'/U_0 along with individual particle locations for $Re_b = 24\,000$ at heights of $x_3^+ = 10$ (left column) and $x_3^+ = 80$ (right column). Top row: $St_K = O(1)$; middle row: $St_K = O(10)$; bottom row: $St_K = O(100)$. Entire horizontal domain is shown and particle sizes are not to scale.

peak production and the walls, in balance with the local TKE production (buffer layer) or transport (viscous sublayer).

Figures 5(g)–5(i) show the particle contribution to TKE for the various Reynolds and Stokes numbers and contain several important features. First, the TKE source due to the dispersed phase can be positive or negative, depending on Stokes number and wall-normal height. At all Reynolds

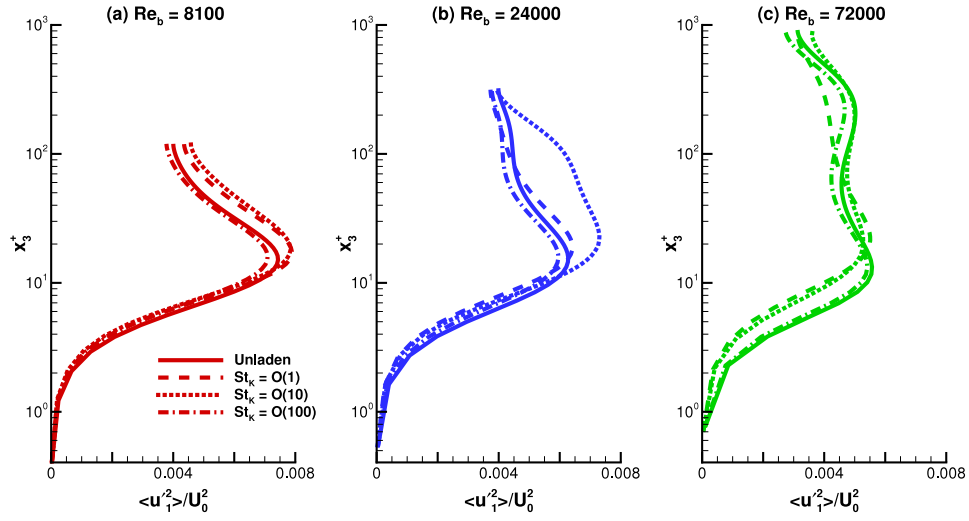

FIG. 3. Same as Figure 1, except for streamwise velocity fluctuation variance $\langle u_1'^2 \rangle / U_0^2$.

numbers, $St_K = O(10)$ and $St_K = O(100)$ particles act as sinks of TKE across the entire domain, peaking in the same general location as TKE production. This is consistent with the idea that heavy, inertial particles inhibit strong turbulent fluctuations by simply acting as obstacles (i.e., through their drag), since the buffer region contains many such turbulent motions, as evidenced by the peak in TKE production. The $St_K = O(1)$ particles, on the other hand, act as a source of TKE throughout the viscous and buffer layers, only becoming a sink at heights greater than $x_3^+ \gtrsim 11$. This is primarily due to their ability to preferentially concentrate in low-speed streaks, where, as they collect into these regions, they lag the fluid on average thus resulting in a positive correlation between the streamwise particle force and velocity fluctuation (that is, the $\langle u_1' F_1 \rangle$ component of Ψ is dominant, confirmed but not shown here. Also see Lee and Lee[46] for a detailed description of this process). The tendency of the $St_K = O(10)$ particles to collect in regions associated with the Couette rollers does not lead to the same behavior of Ψ since, despite a repeated dominance of the streamwise component of Ψ, the additional time history of the more inertial particles leads to a negative correlation between the velocity fluctuations and particle force as they collect in the large-scale, low-speed streaks.

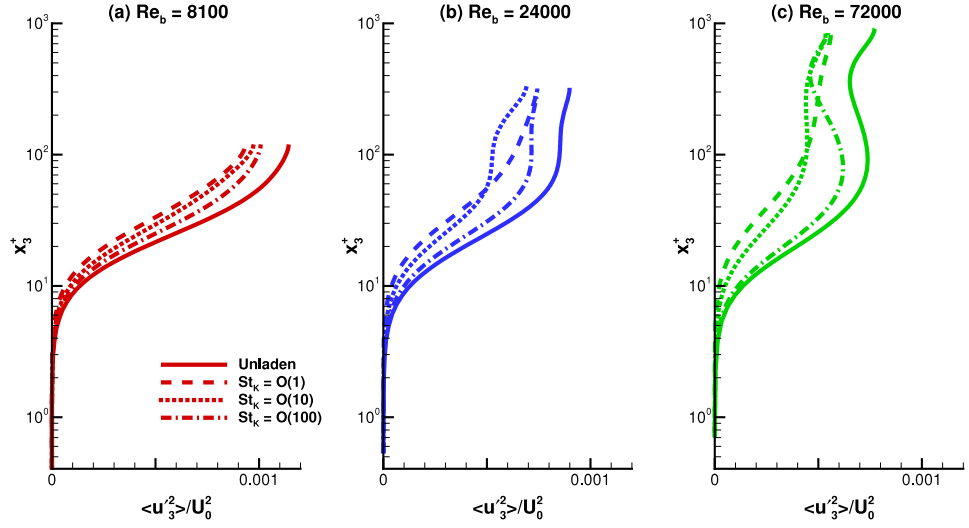

FIG. 4. Same as Figure 1, except for wall-normal velocity fluctuation variance $\langle u_3'^2 \rangle / U_0^2$.

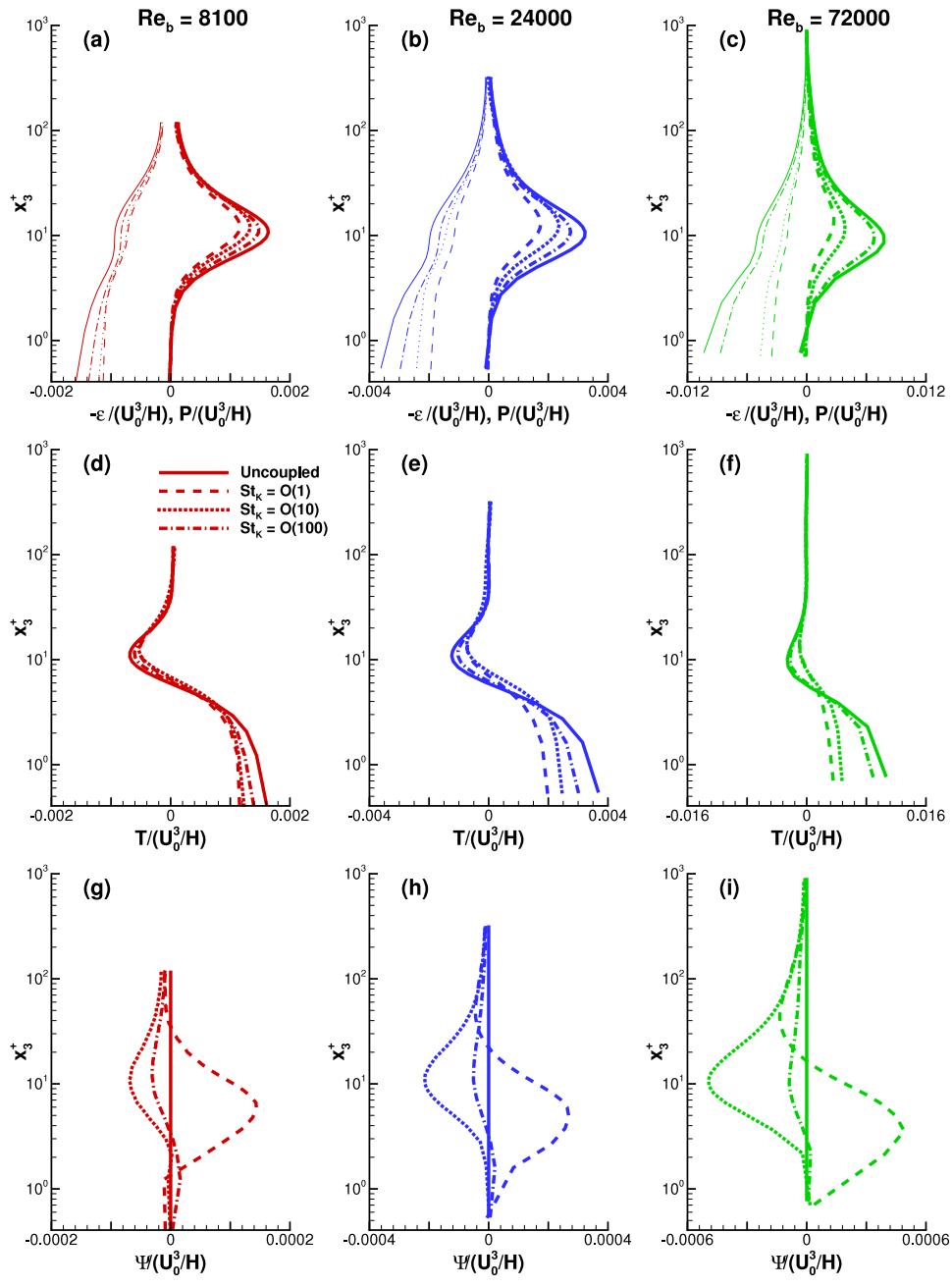

FIG. 5. Components of the TKE budget as given by Equation (22). Different columns correspond to different Reynolds numbers (labeled). Top row (a)-(c) Production $\mathcal{P}$ (thick) and dissipation $-\epsilon$ (thin) of TKE. Middle row (d)-(f) Transport $\mathcal{T}$ of TKE. Bottom row: particle contribution to TKE Ψ. Note the varying scales on the abscissas and the use of logarithmic scaling on the ordinate. Different line types refer to different Stokes numbers, see legend and Figure 1.

More important, however, is the observation that the particle source term is roughly an order of magnitude smaller in comparison with the TKE production, dissipation, and transport, indicating that the particles do not modify turbulence by merely acting as a source or sink of TKE throughout the flow (although the interphase energy transfer can be important for distributing kinetic energy between near-wall and outer-layer regions, see Zhao *et al.*[18]). The direct local influence of Ψ is instead overshadowed by modifications of $\mathcal{P}$, ϵ, and $\mathcal{T}$ with the addition of the dispersed phase, particularly at high Reynolds numbers. TKE production, for example, is dependent upon the Reynolds stress

$\langle u'w' \rangle$, which is widely observed to decrease with the addition of particles.[12,20,23] Therefore, the primary influence of the particles is to decrease the production of TKE, which in turn modifies both TKE transport and dissipation as well. The combined effect on k due to the dispersed phase is seen in Figure 1, which does not necessarily reflect the expected behavior if one only considers the sign of the particle feedback term Ψ.

Generally speaking, the reductions of $\mathcal{P}$, ϵ, and $\mathcal{T}$ are maximized when $St_K = O(1)$ and decrease in magnitude as St_K increases. Again, the reason for this is the maximized ability with which $St_K = O(1)$ particles can preferentially concentrate in regions associated with near-wall hairpins and vortices, thus inhibiting their motion.[32] This dependence of $\mathcal{P}$, ϵ, and $\mathcal{T}$ on St_K is qualitatively different than Ψ, which exhibits altogether different behaviors between $St_K = O(1)$ versus $St_K = O(10)$ or $St_K = O(100)$ particles. More importantly, the magnitude of the decreases of $\mathcal{P}$, ϵ, and $\mathcal{T}$ increases significantly with Reynolds number, indicating that the scale separation between the largest and smallest scales in the flow is playing a large role, and suggesting that particles, despite having diameters smaller than the Kolmogorov scale, are somehow modifying the entire cascade of turbulent kinetic energy, particularly when the range of the cascade becomes large. It also suggests that even at $Re_\tau \approx 900$, these particle-laden flows have not yet reached Reynolds number independence.

B. Spectral energy budgets

Figure 6 presents the kinetic energy modes $\hat{E}_\alpha(k_\alpha)$ as a premultiplied spectra so that the observed area is proportional to the total normalized TKE: $\int_0^\infty k_\alpha \hat{E}_\alpha d(\ln k_\alpha) = k/(L_\alpha/2\pi)$ (recalling that L_α is the domain length in the $\alpha = 1$ or $\alpha = 2$ directions). The spectral decompositions are shown for two different heights: $x_3^+ = 10$ (roughly where the peak in TKE production is found, cf. Figure 5) and $x_3^+ = 80$ (within the logarithmic layer).

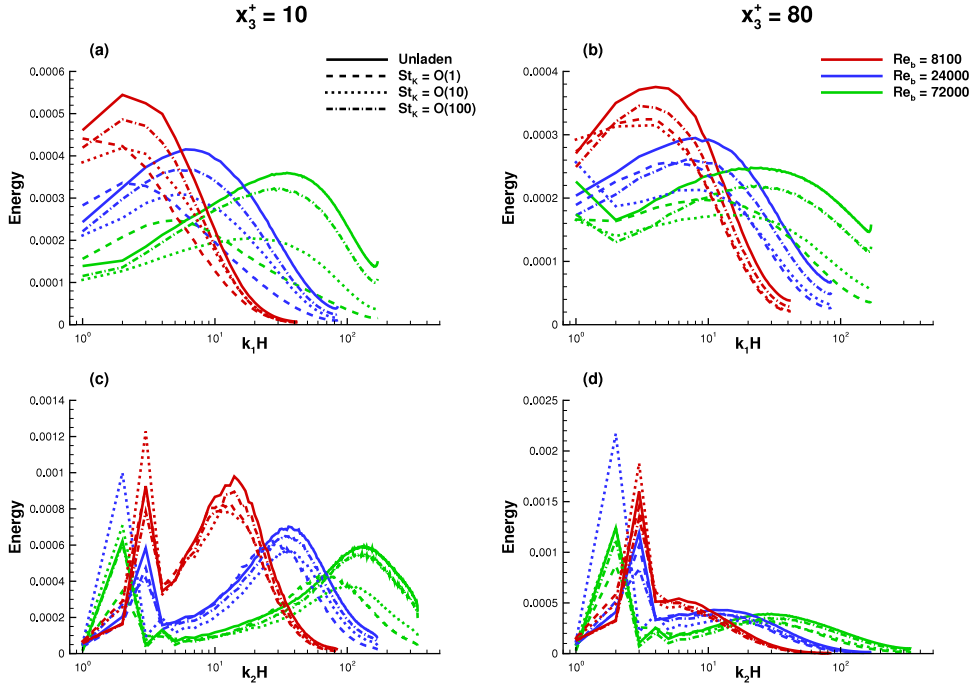

FIG. 6. Premultiplied normalized energy spectra plotted on semilogarithmic axes. Top row (streamwise): $k_1\hat{E}_1/(U_0^2/H)$ versus k_1H; bottom row (spanwise): $k_2\hat{E}_2/(U_0^2/H)$ versus k_2H. Left column: spectra taken at wall-normal height of $x_3^+ = 10$; right column: spectra from $x_3^+ = 80$. Line types indicate various St_K (see legend in panel (a)) while line color refers to various Re_b (see legend in panel (b)).

In Figures 6(a)-6(d), several notable features are found. Starting with Figure 6(a), the lowest Reynolds number shows a near uniform reduction in the energy content of all streamwise modes, with the magnitude of the reduction maximized when $St_K = O(1)$ and decreasing monotonically with increasing St_K (except at the lowest wavenumber). As the Reynolds number increases above $Re_b = 24\,000$, however, particles with $St_K \gtrsim 10$ continue to reduce energy at all streamwise modes, while $St_K = O(1)$ particles exhibit a dual effect: high-wavenumber energy modes are damped while low-wavenumber modes are amplified. Figure 1 shows that the net result is a decrease in the total TKE, which occurs because the high-wavenumber energy reduction is significantly larger than the low-wavenumber amplification. Away from the wall, however, Figure 6(b) shows that this low-wavenumber amplification for $St_K = O(1)$ particles is suppressed, although there is still a wavenumber dependence on the $\hat{E}_1$ reduction that distinctly differs from the more inertial particles. As will be shown later (Figure 8), this wavenumber dependence is due to the direct energy source $\hat{\Psi}$.

Figures 6(c) and 6(d) show the kinetic energy modes taken in the spanwise direction, where the most obvious difference from the streamwise spectral decomposition is the large peak at very low wavenumbers. This peak represents the large-scale Couette rollers, within which the $St_K = O(10)$ particles are susceptible to preferential accumulation. In the logarithmic region ($x_3^+ = 80$), it is clear that these modes contain most of the energy content. Before describing the effects of particles, it must be noted that the limited spanwise domain size and the imposed periodicity influence the location and spectral resolution of these peaks, and that caution must be taken when generalizing their behavior. Ideally, spanwise and streamwise ranges of at least 2-3 times as large should be used to capture converged spectral statistics of these large-scale features. In the tradeoff between achievable domain size and Reynolds number, however, the current study chooses to focus on the effects of Re_b while using a domain width that is assumed to be large enough to capture the essential features of particle interaction with Couette rollers.

Nevertheless, it is clear that the $St_K = O(10)$ particles, at both wall-normal heights, significantly increase the energy content of these roller modes (the shift in the peak wavenumber, for example when $Re_b = 24\,000$, is likely influenced by spanwise periodicity and cannot be claimed as a general result). This enhancement of the roller TKE contribution is less prominent for the largest Reynolds number. For particles with inertial time scales either larger or smaller than the $St_K = O(10)$ particles, the energy contained in these low-wavenumber modes is damped, particularly when $St_K = O(1)$.

At high wavenumbers, the effects of particles are quite similar to that of the streamwise energy modes. Significant reductions in energy content are found at all Re_b and St_K, particularly at high Re_b, with a wavenumber dependence of the reduction magnitude (and slight amplification of $\hat{E}_2$) due to $St_K = O(1)$ particles emerging only at high Reynolds number. Again, this will be argued as resulting from the direct contribution to TKE from the particles.

Overall, the particles tend to reduce the kinetic energy modes across all scales, with two notable exceptions: $St_K = O(1)$ particles have the ability to amplify energy for certain low wavenumbers due to the direct particle TKE source $\hat{\Psi}_\alpha$ (to be shown below), and the preferential accumulation of $St_K = O(10)$ particles results in an increased Couette roller contribution to TKE at low wavenumbers. The low-wavenumber enhancement of energy due to $St_K = O(1)$ particles is almost never strong enough to overshadow the much stronger reductions in $\hat{E}_\alpha$ at higher wavenumbers (thus, $St_K = O(1)$ particles suppress the total TKE at both heights, see Figure 1). The Couette mode enhancement due to $St_K = O(10)$ particles, on the other hand, leads to an increased total TKE for the lower two Re_b cases where this effect is most prominent (i.e., $x_3^+ = 80$). Thus, while nearly all kinetic energy modes are suppressed by the addition of particles, the ability of particles to accumulate in energetic regions (e.g., rollers) or act collectively as clusters (e.g., $St_K = O(1)$ particles) can potentially increase the total TKE in certain regions of the flow.

As described previously, one of the primary emphases of this study is to properly characterize the two-way coupling influence of the particles. Figures 1 and 5 were used above to illustrate that the bulk effects of inertial particles on turbulent kinetic energy in wall-bounded turbulence may not be captured solely by the behavior of the particle feedback term Ψ. Instead, particle-induced changes in TKE production greatly reduce the amount of turbulent kinetic energy that exists throughout the entire cascade, despite the small physical size of the particles themselves.

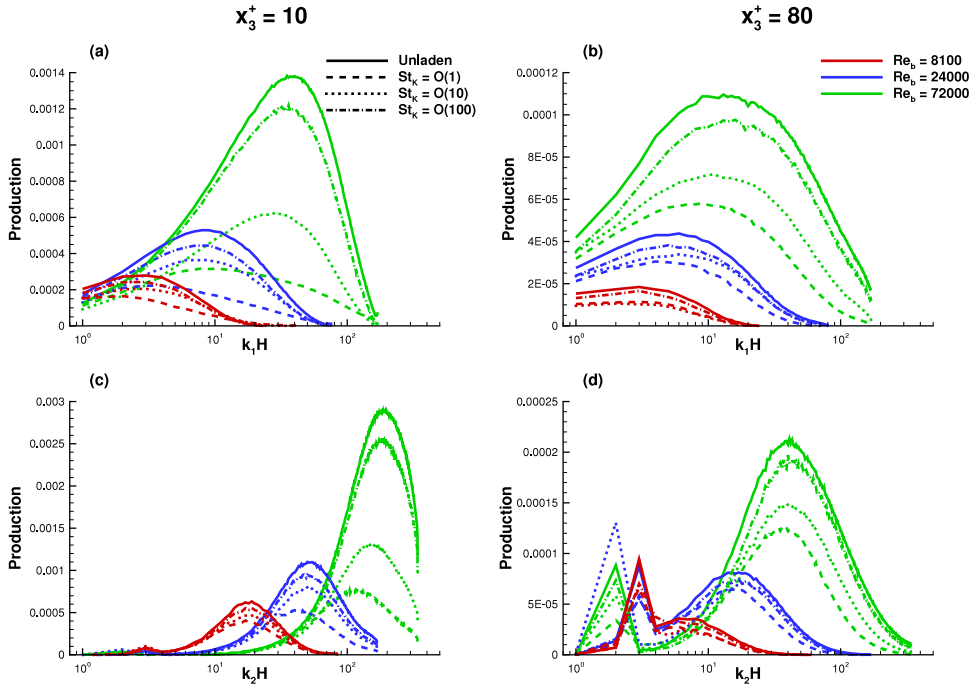

FIG. 7. Premultiplied normalized production spectra plotted on semilogarithmic axes. Top row: $k_1\hat{\mathcal{P}}_1/(U_0^3/H)$ versus k_1H; bottom row: $k_2\hat{\mathcal{P}}_2/(U_0^3/H)$ versus k_2H. Left column: spectra taken at wall-normal height of $x_3^+ = 10$; right column: spectra from $x_3^+ = 80$. Line types indicate various St_K (see legend in panel (a)) while line color refers to various Re_b (see legend in panel (b)).

Figures 7 and 8 therefore show $\hat{\mathcal{P}}_\alpha$ and $\hat{\Psi}_\alpha$, the modal decompositions of TKE production and particle source, respectively, as a function of both streamwise and spanwise wavenumbers. For sake of brevity, the spectral transport $\hat{\mathcal{T}}_\alpha$ and spectral dissipation $\hat{\epsilon}_\alpha$ are not shown, since the behavior of $\hat{\mathcal{P}}_\alpha$ and $\hat{\Psi}_\alpha$ is found to illustrate the most important details of particle-induced modifications to the TKE budget. Note that it is generally true that the changes to spectral dissipation mirror the behavior of $\hat{\mathcal{P}}_\alpha$. As before, the quantities $\hat{\mathcal{P}}_\alpha$ and $\hat{\Psi}_\alpha$ are plotted in a way such that the observed area is proportional to the total production $\mathcal{P}$ and particle source Ψ.

The underlying tendency of particles to damp turbulent kinetic energy across all modes (Figure 6) is seen in Figures 7(a)-7(d) as resulting from the near broadband reduction of $\hat{\mathcal{P}}_1$ and $\hat{\mathcal{P}}_2$ across all wavenumbers. For high Reynolds numbers, this reduction is quite large, both in terms of $\hat{\mathcal{P}}_1$ and $\hat{\mathcal{P}}_2$. The only exception to this broadband reduction is for $\hat{\mathcal{P}}_2$ at $x_3^+ = 80$ at wavenumbers associated with the Couette rollers at $Re_b = 24\,000$, in agreement with Figure 1(b).

It is important to note that the strong reduction of $\hat{\mathcal{P}}_\alpha$ is sensitive to particle Stokes number only insomuch that St_K determines the magnitude of the reduction and not necessarily the spectral range where it occurs. Thus, differences in the preferential accumulation tendencies of particles with different inertias apparently alter the magnitude of TKE production but not the spectral location of this interaction. This is true for both spanwise and streamwise production modes $\hat{\mathcal{P}}_1$ and $\hat{\mathcal{P}}_2$. In Richter and Sullivan,[32] it is argued that this difference in efficiency is directly related to the ability of particles to collect in ejection regions (and thus regions of high Reynolds stress) near the wall. The wavenumber dependence of the particle-induced changes in $\hat{E}_\alpha$ seen above in Figure 6, for example when $St_K = O(1)$ at high wavenumbers near the wall, is instead a result of the direct particle contribution $\hat{\Psi}_\alpha$.

This is clearly seen in Figure 8, which shows that the particle energy source $\hat{\Psi}_\alpha$ generally has a strong wavenumber dependence which is highly sensitive to St_K. For streamwise modes ($\hat{\Psi}_1$, Figures 8(a) and 8(b)), $St_K = O(1)$ particles at all Reynolds numbers act as a direct energy sink at high wavenumbers while acting as a source at low wavenumbers. This behavior is most obvious

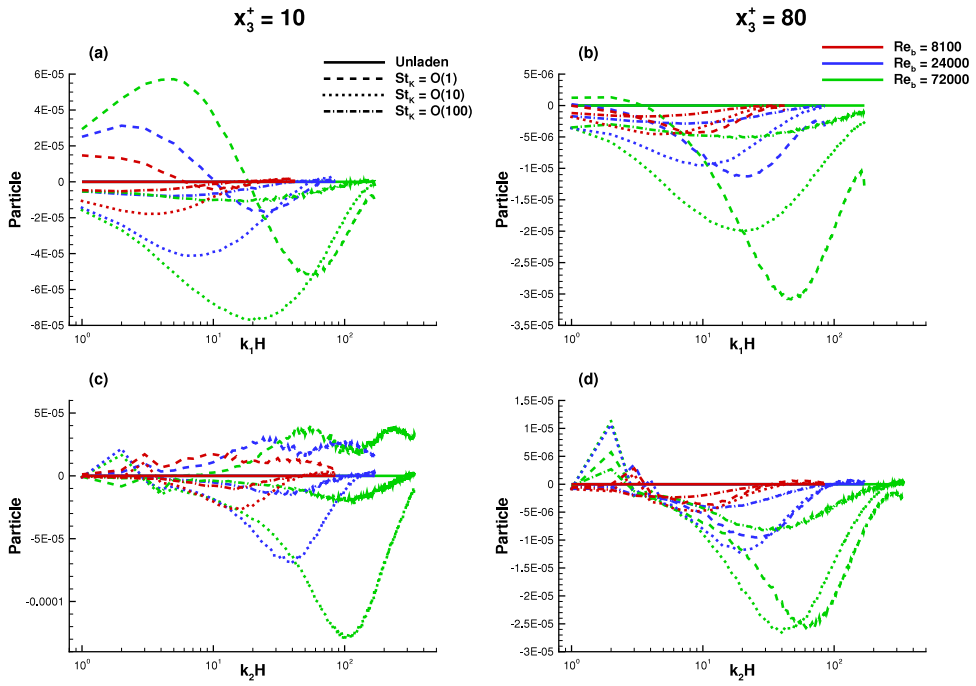

FIG. 8. Premultiplied normalized particle source spectra plotted on semilogarithmic axes. Top row: $k_1\hat{\Psi}_1/(U_0^3/H)$ versus k_1H; bottom row: $k_2\hat{\Psi}_2/(U_0^3/H)$ versus k_2H. Left column: spectra taken at wall-normal height of $x_3^+ = 10$; right column: spectra from $x_3^+ = 80$. Line types indicate various St_K (see legend in panel (a)) while line color refers to various Re_b (see legend in panel (b)).

at the $x_3^+ = 10$ location. While the wavenumber dependence of $\hat{\Psi}_\alpha$ is in some ways similar to the DNS results of Gualtieri *et al.*[33] and modeling analysis of Druzhinin[34] for $St_K \approx 1$, the overall behavior found in the present case is actually opposite: both Gualtieri *et al.*[33] and Druzhinin[34] find a direct particle sink of TKE at low wavenumbers and a source of TKE at high wavenumbers when $St_K \approx 1$, highlighting the fundamental differences in two-way coupling between wall-bounded and homogeneous turbulent flows. For instance, the homogeneous shear flow simulations of Gualtieri *et al.*[33] show that the streamwise component of their particle coupling term acts as a source at low wavenumbers, but that this is overwhelmed by the TKE extraction of the other two components at the same low wavenumbers (their Figures 14 and 15). In the present case, this streamwise source component dominates and ultimately manifests itself as a direct particle source at low wavenumbers, likely due to particle clustering within near-wall low-speed streaks.

The ability of $St_K = O(1)$ particles to act as a direct source of TKE at low wavenumbers and a sink of TKE at high wavenumbers is in stark contrast to particles with $St_K = O(10)$, which act as sinks of TKE throughout the entire wavenumber range. $St_K = O(100)$ particles also act as direct sinks throughout all available streamwise wavenumbers, but their lack of preferential concentration makes this contribution very small.

Figures 8(c) and 8(d) show similar behavior when considering spanwise modes, in that $St_K = O(1)$ particles act quite differently compared to more inertial particles, particularly at the near-wall location. At $x_3^+ = 10$, $St_K = O(1)$ particles now act as a source of TKE at nearly all spanwise wavenumbers while more inertial particles act as sinks. As for the streamwise modes near the wall, the magnitude of $\hat{\Psi}_2$ is largest for the $St_K = O(10)$ particles. In the logarithmic region, the three different Stokes numbers behave similarly at high wavenumber (with various magnitudes of $\hat{\Psi}_2$), while it is clear that, again, $St_K = O(10)$ particles tend to act as a source of TKE at the low wavenumbers associated with the Couette rollers. At the highest Reynolds number, all particles act as a source of TKE at these low wavenumbers.

C. Discussion

As mentioned above, it is well-established[45,48] that particles preferentially concentrate relative to motions associated with their own acceleration time scale. Recall that for the definition of St_K used presently, the $St_K = O(1)$ particles collect in small-scale high- and low-speed streak regions near the wall, $St_K = O(10)$ particles collect instead in regions associated with the Couette rollers due to their larger inertia, and $St_K = O(100)$ particles experience relatively little preferential concentration (see Figure 2). At the same time, Figures 7 and 8 show that there are two distinct routes through which particles can modify the turbulent cascade of kinetic energy: (1) a broadband reduction of $\hat{\mathcal{P}}_\alpha$ which is only sensitive to St_K in regards to the magnitude of the reduction, with no strong wavenumber dependence and (2) a direct particle energy exchange $\hat{\Psi}_\alpha$ which has a wavenumber dependence which changes significantly based on St_K. While the former is primarily a result of a broad damping of wall-normal velocity fluctuations (e.g., Figure 4, consequently lowering the Reynolds stress), the latter is dependent on the degree and scale of preferential concentration and primarily affects the behavior of streamwise velocity fluctuations (e.g., Figure 3).

Figure 9 shows a normalized power spectral density (PSD) of the mass concentration fluctuation: $\frac{\langle \hat{c}'\hat{c}'^* \rangle}{\langle c'^2 \rangle}$. This is provided both as a function of both streamwise (top) and spanwise (bottom) wavenumbers, where $\hat{c}'$ is the Fourier coefficient of the concentration fluctuation (via Equations (7) or (8)), and $\langle c'^2 \rangle$ is the height-dependent concentration fluctuation variance, which is related to the Fourier coefficients in a way similar to Equation (11),

$$\langle c'^2 \rangle (x_3) = \sum_{k_1} \langle \hat{c}'\hat{c}'^* \rangle (k_1, x_3) = \sum_{k_2} \langle \hat{c}'\hat{c}'^* \rangle (k_2, x_3), \tag{23}$$

where parentheses reflect a functional dependence. Here, the Eulerian concentration field is computed by summing all particle masses in a grid cell and dividing by the cell volume, and thus, the highest wavenumber which can be represented in the PSD is limited by the modes which the Eulerian grid can represent.

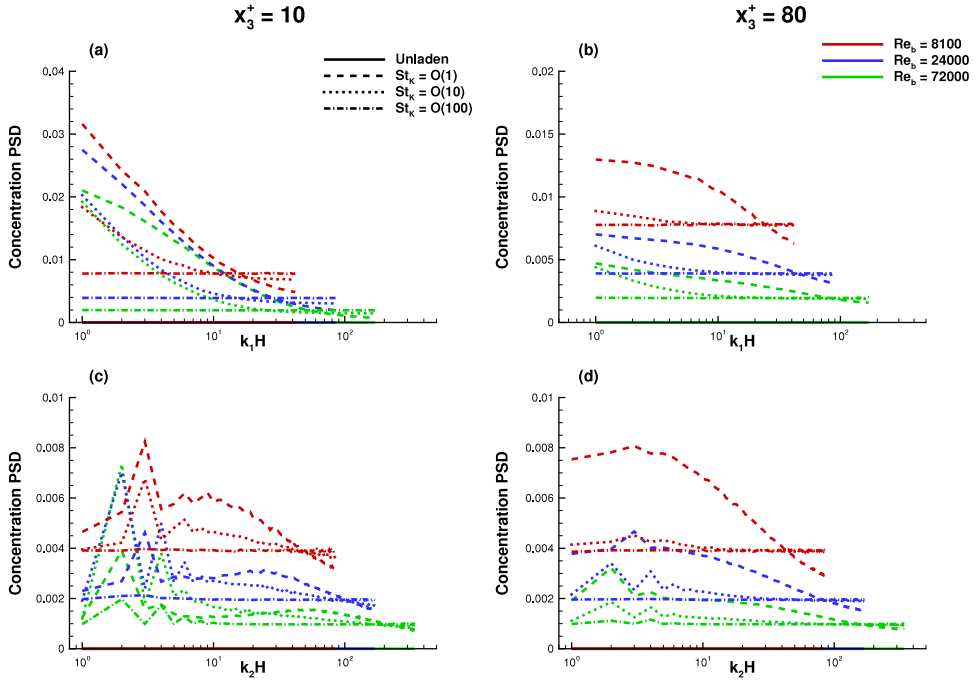

FIG. 9. Power spectral density of the particle mass concentration fluctuation field, normalized by the fluctuation variance at the local height, $\frac{\langle \hat{c}'^*\hat{c}' \rangle}{\langle c'^2 \rangle}$, plotted as a function of streamwise (top row) or spanwise (bottom row) wave numbers k_1 and k_2. As in other plots, colors refer to Re_b, line types refer to St_K (see legends). Left column taken from $x_3^+ = 10$ and right column taken from $x_3^+ = 80$.

Figure 9 therefore represents the concentration fluctuation energy contained at each wavenumber in either the streamwise or spanwise direction, again shown for heights near the peak of energy production ($x_3^+ = 10$) and within the logarithmic region ($x_3^+ = 80$). The trends quantitatively confirm the general behavior seen in the snapshots of Figure 2: elongated, streamwise-oriented structures of preferential concentration (where it exists) lead to low wavenumber content for streamwise modes and one or more peaks at low and intermediate wavenumbers for the spanwise modes. Near the wall, this behavior is more pronounced.

In general, the concentration fields associated with $St_K = O(1)$ particles contain a wider range of wavenumber content due to their ability to collect in small-scale regions, and this is true at all Re_b and at both heights. For the streamwise modes (top row), the maximum of the PSD occurs at the lowest wavenumbers. For the spanwise modes (bottom row), a peak exists at all Re_b corresponding to the Couette rollers, with a smaller, broader secondary peak at higher wavenumbers. This secondary peak corresponds to the small-scale preferential concentration exhibited by $St_K = O(1)$ particles and indicates that these clusters exist over a broad range of spanwise scales. At $x_3^+ = 80$, the streakiness of the particle accumulation decreases significantly (see Figure 2), and therefore, a closer similarity between the streamwise and spanwise PSD structures exists at all Re_b (right column).

For $St_K = O(10)$ particles, again the images of Figure 2 are confirmed. At both heights, the streamwise PSD modes are maximized at the lowest wavenumbers (associated with long, straight concentration streaks), with a much steeper decrease with increasing k_1 than the $St_K = O(1)$ particles. The spanwise PSD modes confirm that the particles tend to align in the regions associated with Couette rollers, with no secondary peak as with the $St_K = O(1)$ particles. For $St_K = O(100)$ particles, there is almost no wavenumber dependence of the concentration fluctuation field at any height or at any Re_b, indicating that these particles remain homogeneously distributed, except for a minor influence of the Couette rollers at the highest Reynolds number. The near-horizontal line for $St_K = O(100)$ particles therefore represents the average PSD magnitude for all other St_K curves at the same Re_b since the normalization ensures that the integrals are the same.

The most important feature of Figure 9, however, is its relation to both the production spectra $\hat{\mathcal{P}}_\alpha$ and the particle feedback term $\hat{\Psi}_\alpha$ seen in figures 7 and 8. As described above, the shear production shown in Figures 5(a)-5(c) was found to be reduced significantly at nearly all wavenumbers (Figure 7). The effect of St_K was only to roughly determine the magnitude of this reduction, with the $St_K = O(1)$ particles exhibiting the largest reduction at all Re_b. At the same time, certain regions of the streamwise and spanwise energy modes were found to experience a highly wavenumber-dependent modification, whose location was sensitive to St_K. This was found to result from the smaller-in-magnitude particle feedback term $\hat{\Psi}_\alpha$ (Figure 8).

By inspecting the trends in Figure 9, loose connections can be made between the particle exchange term $\hat{\Psi}_\alpha$ and the modes containing more concentration fluctuation energy. Most obviously, the significant dependence of the shape of $\hat{\Psi}_\alpha$ on St_K at both wall-normal heights gives evidence that the particle exchange term is highly susceptible to preferential concentration, which Figure 9 partially quantifies. While there are no distinct one-to-one features which exist in the concentration PSD whose direct effect can be found in the $\hat{\Psi}_\alpha$ spectra, general features exist which gently indicate that there is a connection between the two (which is perhaps unsurprising[33]). Near the wall, for example, Figure 7(a) shows that the $St_K = O(1)$ particles act to extract energy at small scales while providing a source of TKE at large scales. The transition from energy amplification to energy extraction occurs at a wavenumber closely corresponding to the location where the mass concentration PSD drops below the average level (i.e., that exhibited by the $St_K = O(100)$ particles). Similarly, the first of the two positive peaks found in Figure 9(c) at high wavenumbers for $St_K = O(1)$ particles is found to roughly correlate with the wavenumber location of the secondary peak in the concentration PSD. The second high wavenumber peak corresponds to the location where the concentration PSD goes below the average level.

Assuming that the spanwise concentration PSD provides more insight into the ability to preferentially concentrate (since the small streaks are oriented in the streamwise direction), Figures 8(c) and 9(c) indicate that a secondary peak in the concentration fluctuation PSD for $St_K = O(1)$ is concurrent with a positive TKE source at slightly higher wavenumbers. This suggests that the

preferential concentration of these $St_K = O(1)$ particles enables them to act as a source of energy at high spanwise modes by acting collectively — consistent with the increase of $\langle u'^2 \rangle$ due to the strengthening of low-speed streaks — whereas the larger particles act even more strongly as a sink at the same spanwise wavenumbers since they merely act as independent sources of dissipation.

IV. CONCLUSIONS

Two-way coupled simulations of turbulent Couette flow were performed using DNS of the carrier phase and the standard Lagrangian point-particle approximation for the dispersed phase. At a constant dispersed phase mass fraction of $\phi_m = 0.25$, simulations of three different magnitudes of particle Stokes number ($St_K = [O(1), O(10), O(100)]$) were performed at three increasingly large Reynolds numbers: $Re_b = [8100, 24\,000, 72\,000]$ (corresponding to friction Reynolds numbers of approximately $[125, 325, 900]$). The focus of this study was to observe and interpret the spectral distribution of the key terms of the turbulent kinetic energy budget, with the hopes of better understanding how particles modify turbulent kinetic energy in wall-bounded flows in order to aid and inform model development.

It is shown that the aggregate behavior of TKE is a complex function of wall-normal height, Stokes number, and Reynolds number, and that the individual components of k (namely, the streamwise and wall-normal velocity fluctuations) are affected differently by the presence of inertial particles. Low-speed streaks at the wall can be strengthened if preferential accumulation of particles occurs, while wall-normal velocity fluctuations are universally damped. This leads to increased k in some regions of the flow with decreases of k in others.

When inspecting the TKE budget, it is found that particles significantly reduce turbulent shear production, and that this reduction occurs across nearly all spanwise and streamwise wavenumber modes. At the same time, the direct particle contribution to the TKE budget is an order of magnitude smaller than other terms in the TKE budget but has the ability to modify the wavenumber dependence of the total kinetic energy. In some regions of wavenumber space (e.g., the Couette rollers), particles can enhance TKE directly.

Physically, a picture develops which can be described as follows. Particles have two simultaneous effects in this wall-bounded turbulent flow: (1) a broadband reduction of TKE production in wavenumber space, where St_K only has the effect of modifying the magnitude of this reduction and (2) a direct particle contribution which is tightly linked to preferential concentration, where the collective effects of particle clusters can directly influence TKE content at different wavenumbers.

For $St_K = O(1)$ particles, this effect is most pronounced because these particles have the maximum ability to collect into small-scale regions. This preferential accumulation leads to a very large reduction of TKE production at all wavenumbers, while having the dual effect of increasing modal energy content at low wavenumbers due to the collective action of the particles. $St_K = O(10)$ particles exhibit similar behavior, though their preferential concentration is confined only to the large-scale rollers since their inertia is too large to collect among the small-scale hairpin vortices.[32] Their direct interaction therefore comes mostly at the scales associated with the Couette rollers, while their influence on production remains broadband.

This general picture suggests that any model of turbulence modulation must capture two distinct features at the same time. The first is much simpler, since the reduction in production is likely a result of the severe damping of the wall-normal velocity fluctuations. As shown in Richter and Sullivan,[32] $St_K = O(1)$ particles collect precisely in the regions associated with turbulent ejections from the wall, which maximizes their ability to modify wall-normal velocity fluctuations. The only effect of St_K in this process is to change the efficiency of this process — the actual time history of the particle appears to have no direct influence. A crude model based, for example, merely on artificially damping vertical fluctuations based on local particle concentrations works well in reproducing the general trend of production reduction (not shown here).

The direct particle feedback, on the other hand, is tightly linked to the preferential concentration of the particles and thus is a complex function of St_K since the time history of the particles becomes important. The particles act collectively to modify turbulence, which can manifest itself as

either a source or sink. In many regions of the flow, this effect is much smaller in magnitude than the changes in TKE production, but the spectral distribution of energy can be modified significantly even if the total energy is identical. It is this feature of particle-laden flows which appears to pose the largest challenge to bulk-scale modeling.

Finally, the similarity between particle-induced turbulence modification and viscoelastic turbulence must be noted. In both cases, the presence of a constituent (either particles or polymer molecules) which is much smaller in size than any of the turbulent motions may have inherent dynamical time scales which can approach or even exceed those found in the turbulence (indicated by the Stokes number in the present case and by the Deborah or Weissenberg number for the case of polymer additives). It has been argued that due to the matching of time scales, small polymers, despite their small size, can *directly* interact with large-scale structures and impede their motions. Recently, Valente *et al.*[49] find what they describe as a "polymer-induced energy cascade," where energy is directly extracted from large scales and either dissipated by the polymers themselves or given back to the flow to be dissipated by viscous motions.

In the present context, it is helpful to recall the original motivation for this study: can small particles collectively modify motions across all turbulent scales, or is there perhaps an upscale effect that allows them to modify the entire cascade of TKE? While not definitive, the present results hint at the presence of both: i.e., particle clustering (which does not have an analog in the viscoelastic case) can provide an St_K-dependent energy source/sink which varies with wavenumbers associated with the clusters themselves. The signs of this direct influence (Figure 8(a)) suggest that an upscale energy transfer may be occurring in this process. At the same time, a small-scale damping of vertical velocity fluctuations is sufficient to induce a reduction in turbulent production throughout the entire energy cascade. Meanwhile, attempts at understanding TKE content of the dispersed phase rather than the carrier phase have shown the importance of distinguishing between random, uncorrelated motions (those caused by a strong time history) and correlated motions of particles (those caused by local processes such as collisions or low Stokes numbers) (e.g., Février *et al.*[50] and Fox[51]), which may possibly be related to the two coupling processes outlined here. Only by continuing to study the dynamics of these inertial particles in two-way coupled flows, however, can the picture be fully developed.

ACKNOWLEDGMENTS

The author is grateful to the Computational and Information Systems Laboratory (CISL) of the National Center for Atmospheric Research, who provided the computational resources for the simulations presented through the Accelerated Scientific Discovery program. The author would also like to thank the Computing Research Center at the University of Notre Dame for computational support and access to local resources.

[1] T. Tanaka and J. K. Eaton, "Classification of turbulence modification by dispersed spheres using a novel dimensionless number," Phys. Rev. Lett. **101**, 114502 (2008).
[2] R. A. Gore and C. T. Crowe, "Effect of particle size on modulating turbulent intensity," Int. J. Multiphase Flow **15**(2), 279–285 (1989).
[3] S. Elghobashi, "On predicting particle-laden turbulent flows," Appl. Sci. Res. **52**(4), 309–329 (1994).
[4] W. Hwang and J. K. Eaton, "Homogeneous and isotropic turbulence modulation by small heavy (St ~ 50) particles," J. Fluid Mech. **564**, 361–393 (2006).
[5] S. Geiss, A. Dreizler, Z. Stojanovic, M. Chrigui, A. Sadiki, and J. Janicka, "Investigation of turbulence modification in a non-reactive two-phase flow," Exp. Fluids **36**, 344–354 (2004).
[6] S. Schreck and S. J. Kleis, "Modification of grid-generated turbulence by solid particles," J. Fluid Mech. **249**, 665–688 (1993).
[7] T. S. Yang and S. S. Shy, "Two-way interaction between solid particles and homogeneous air turbulence: Particle settling rate and turbulence modification measurements," J. Fluid Mech. **526**, 171–216 (2005).
[8] G. Bellani, M. L. Byron, A. G. Collignon, C. R. Meyer, and E. A. Variano, "Shape effects on turbulent modulation by large nearly neutrally buoyant particles," J. Fluid Mech. **712**, 41–60 (2012).
[9] J. D. Kulick, J. R. Fessler, and J. K. Eaton, "Particle response and turbulence modification in fully developed channel flow," J. Fluid Mech. **277**, 109–134 (1994).
[10] N. Caraman, J. Borée, and O. Simonin, "Effect of collisions on the dispersed phase fluctuation in a dilute tube flow: Experimental and theoretical analysis," Phys. Fluids **15**, 3602 (2003).

[11] M. Rashidi, G. Hetsroni, and S. Banerjee, "Particle-turbulence interaction in a boundary layer," Int. J. Multiphase Flow **16**(6), 935–949 (1990).
[12] M. Righetti and G. P. Romano, "Particle-fluid interactions in a plane near-wall turbulent flow," J. Fluid Mech. **505**, 93–121 (2004).
[13] Y. Tsuji, Y. Morikawa, and H. Shiomi, "LDV measurements of an air-solid two-phase flow in a vertical pipe," J. Fluid Mech. **139**, 417–434 (1984).
[14] S. Elghobashi and G. C. Truesdell, "On the two-way interaction between homogeneous turbulence and dispersed solid particles. I: Turbulence modification," Phys. Fluids A **5**, 1790 (1993).
[15] K. D. Squires and J. K. Eaton, "Measurements of particle dispersion obtained from direct numerical simulations of isotropic turbulence," J. Fluid Mech. **226**, 1–35 (1991).
[16] A. Ferrante and S. Elghobashi, "On the physical mechanisms of two-way coupling in particle-laden isotropic turbulence," Phys. Fluids **15**(2), 315–329 (2003).
[17] S. Sundaram and L. R. Collins, "A numerical study of the modulation of isotropic turbulence by suspended particles," J. Fluid Mech. **379**, 105–143 (1999).
[18] L. Zhao, H. I. Andersson, and J. J. J. Gillissen, "Interphasial energy transfer and particle dissipation in particle-laden wall turbulence," J. Fluid Mech. **715**, 32–59 (2013).
[19] L. Zhao, H. I. Andersson, and J. J. J. Gillissen, "Turbulence modulation and drag reduction by spherical particles," Phys. Fluids **22**, 081702 (2010).
[20] A. W. Vreman, "Turbulence characteristics of particle-laden pipe flow," J. Fluid Mech. **584**, 235–279 (2007).
[21] Y. Mito and T. J. Hanratty, "Effect of feedback and inter-particle collisions in an idealized gas-liquid annular flow," Int. J. Multiphase Flow **32**, 692–716 (2006).
[22] Y. Li, J. B. McLaughlin, K. Kontomaris, and L. Portela, "Numerical simulation of particle-laden turbulent channel flow," Phys. Fluids **13**(10), 2957–2967 (2001).
[23] D. H. Richter and P. P. Sullivan, "Momentum transfer in a turbulent, particle-laden Couette flow," Phys. Fluids **25**, 053304 (2013).
[24] F. Lucci, A. Ferrante, and S. Elghobashi, "Is Stokes number an appropriate indicator for turbulence modulation by particles of Taylor-length-scale size?," Phys. Fluids **23**, 025101 (2011).
[25] H. Gao, H. Li, and L.-P. Wang, "Lattice Boltzmann simulation of turbulent flow laden with finite-size particles," Comput. Math. Appl. **65**, 194–210 (2013).
[26] M. Uhlmann and T. Doychev, "Sedimentation of a dilute suspension of rigid spheres at intermediate Galileo numbers: The effect of clustering upon the particle motion," J. Fluid Mech. **752**, 310–348 (2014).
[27] S. Tenneti and S. Subramaniam, "Particle-resolved direct numerical simulation for gas-solid flow model development," Annu. Rev. Fluid Mech. **46**, 199–230 (2014).
[28] C. D. Dritselis and N. S. Vlachos, "Numerical study of educed coherent structures in the near-wall region of a particle-laden channel flow," Phys. Fluids **20**, 055103 (2008).
[29] C. Poelma and G. Ooms, "Particle-turbulence interaction in a homogeneous, isotropic turbulent suspension," Appl. Mech. Rev. **59**(2), 78–90 (2006).
[30] C. B. Rogers and J. K. Eaton, "The effect of small particles on fluid turbulence in a flat-plate, turbulent boundary layer in air," Phys. Fluids A **3**, 928 (1991).
[31] Y. Yamamoto, M. Potthoff, T. Tanaka, T. Kajishima, and Y. Tsuji, "Large-eddy simulation of turbulent gas-particle flow in a vertical channel: Effect of considering inter-particle collisions," J. Fluid Mech. **442**, 303–334 (2001).
[32] D. H. Richter and P. P. Sullivan, "Modification of near-wall coherent structures by inertial particles," Phys. Fluids **26**, 103304 (2014).
[33] P. Gualtieri, F. Picano, G. Sardina, and C. M. Casciola, "Clustering and turbulence modulation in particle-laden shear flows," J. Fluid Mech. **715**, 134–162 (2013).
[34] O. A. Druzhinin, "The influence of particle inertia on the two-way coupling and modification of isotropic turbulence by microparticles," Phys. Fluids **13**, 3738 (2001).
[35] M. R. Maxey and J. J. Riley, "Equation of motion for a small rigid sphere in nonuniform flow," Phys. Fluids **26**(4), 883–889 (1983).
[36] P. R. Spalart, R. D. Moser, and M. M. Rogers, "Spectral methods for the Navier-Stokes equations with one infinite and two periodic directions," J. Comput. Phys. **96**, 297–324 (1991).
[37] V. Armenio and V. Fiorotto, "The importance of the forces acting on particles in turbulent flows," Phys. Fluids **13**, 2437 (2001).
[38] R. Clift, J. R. Grace, and M. E. Weber, *Bubbles, Drops, and Particles* (Academic Press, 1978).
[39] S. Sundaram and L. R. Collins, "Numerical considerations in simulating a turbulent suspension of finite-volume particles," J. Comput. Phys. **124**(2), 337–350 (1996).
[40] J. Komminaho, A. Lundbladh, and A. V. Johansson, "Very large structures in plane turbulent Couette flow," J. Fluid Mech. **320**, 259–285 (1996).
[41] T. Tsukahara, H. Kawamura, and K. Shingai, "DNS of turbulent Couette flow with emphasis on the large-scale structure in the core region," J. Turbul. **7**(19), 1–16 (2006).
[42] I. A. Bolotnov, R. T. Lahey, Jr., D. A. Drew, K. E. Jansen, and A. A. Oberai, "Spectral analysis of turbulence based on the DNS of a channel flow," Comput. Fluids **39**, 640–655 (2010).
[43] J. A. Domaradzki, W. Liu, C. Hartel, and L. Kleiser, "Energy transfer in numerically simulated wall-bounded turbulent flows," Phys. Fluids **6**, 1583 (1994).
[44] S. B. Pope, *Turbulent Flows* (Cambridge University Press, Cambridge, UK, 2000), ISBN: 978-0-521-599886-6.
[45] D. W. I. Rouson and J. K. Eaton, "On the preferential concentration of solid particles in turbulent channel flow," J. Fluid Mech. **428**, 149–169 (2001).
[46] J. Lee and C. Lee, "Modification of particle-laden near-wall turbulence: Effect of Stokes number," Phys. Fluids **27**, 023303 (2015).

[47] A. J. Smits, B. J. McKeon, and I. Marusic, "High-Reynolds number wall turbulence," Annu. Rev. Fluid Mech. **43**, 353–375 (2011).
[48] J. Bec, L. Biferale, M. Cencini, A. Lanotte, S. Musacchio, and F. Toschi, "Heavy particle concentration in turbulence at dissipative and inertial scales," Phys. Rev. Lett. **98**, 084502 (2007).
[49] P. C. Valente, C. B. da Silva, and F. T. Pinho, "The effect of viscoelasticity on the turbulent kinetic energy cascade," J. Fluid Mech. **760**, 39–62 (2014).
[50] P. Février, O. Simonin, and K. D. Squires, "Partitioning of particle velocities in gas-solid turbulent flows into a continuous field and a spatially uncorrelated random distribution: Theoretical formalism and numerical study," J. Fluid Mech. **533**, 1–46 (2005).
[51] R. O. Fox, "On multiphase turbulence models for collisional fluid-particle flows," J. Fluid Mech. **742**, 368–424 (2014).